SEMI-TRANSPARENT ZnO:Al/Cu_2O THIN-FILM HETEROJNCTION FBRICATED AT LOW TEMPERATURE: EFFECT OF AN INTRINSIC ZnO BUFFER LAYER AT THE JUNCTION

by

YU NUNG HUANG

Presented to the Faculty of the Graduate School of

The University of Texas at Arlington in Partial Fulfillment

of the Requirements

for the Degree of

MASTER OF SCIENCE IN MATERIALS SCIENCE AND ENGINEERING

THE UNIVERSITY OF TEXAS AT ARLINGTON

December 2011

ACKNOWLEDGEMENTS

It is truly an honor for me to have Dr. Yaowu Hao and Dr. Fuqiang Liu to be my committee members. Their participation made this thesis better-rounded. I sincerely appreciate my academic advisor, Dr. Michael Jin made this thesis possible and has made his support available in a number of ways. He has taught me in all the aspects of doing research and writing this thesis. Without him to point out the right direction and share the professionalism, I cannot achieve it.

I acknowledged the help of Dr. Jiechao Jiang and David Yan from The UTA Characterization Center for Materials and Biology. They have provided me trainings for utilizing facilities. I am indebted to my colleagues to support me for all the aspects in doing experiments. We made a great team. I have learned so much from Mr. Soo Kim, Mr. Erkan Mehmet Eray, Mr. Daniel Wu, and Mrs. Ameena Fnu when we worked together. I also benefited from the expertise and technical supports from Mr. Mcnatt, Jeremiah S of NASA Glenn Research Center. The direction he has been shared with me was very valuable to the project.

In addition, I have received administrative support from the staff out of Materials Science & Engineering Department, Mrs. Jennifer Standlee and Mrs. Libia Cuauhtli, for processing the department scholarship and graduation application for me. On a special note, I would like to thank Dr. Wen S. Chan from Mechanical & Aerospace Engineering Department and Dr. Jeff Tsay from Department of Accounting for kindly sharing their precious life experiences and board knowledge during my time with UTA Taiwanese student association.

The last but not the least, my special thanks go to my mother, Mrs. Shu-Chu Liou, and my friend, Ms. Hsiao-Yi Kuo. Without their full support for my personal life, I would not be myself and accomplish my master degree.

November 10, 2011

ABSTRACT

SEMI-TRANSPARENT ZnO:Al/Cu_2O THIN-FILM HETEROJNCTION FBRICATED AT LOW TEMPERATURE: EFFECT OF AN INTRINSIC ZnO BUFFER LAYER AT THE JUNCTION

YU NUNG HUANG

The University of Texas at Arlington, 2011

Supervising Professor: Michael Jin

The Al-doped ZnO (AZO)/Cu_2O semi-transparent heterojunction was realized by an RF sputtering at low temperature in this study. Specifically, the usage of a buffer layer in the junction structure has been found as a key factor influencing the carrier transport mechanisms and performance of the junction. First, the chemical bath deposition (CBD) has been utilized in depositing an intrinsic ZnO (i-ZnO) buffer layer in order to entirely avoid potential plasma damage from a subsequent sputter deposition process. Increasing pH of CBD solution was critical in delaying the formation of detrimental $ZnOH_x$ particles in the solution and the assistance of ultrasonication improved the uniformity of i-ZnO further by minimizing the adherence of $ZnOH_x$ particles on the growing surface of i-ZnO. The deposition of i-ZnO buffer layer on top of AZO prior to the sputter deposition of Cu_2O produced rectifying junctions by reducing the tunneling of charge carriers through interface defects at the junction. Yet, it is concluded that the presence of the defects at the junction cannot be avoided due to the lattice mismatch between Cu_2O and ZnO limiting the performance of the device intrinsically.

TABLE OF CONTENTS

ACKNOWLEDGEMENTS……iii

ABSTRACT……iv

LIST OF ILLUSTRATIONS……viii

LIST OF TABLES……xi

LIST OF SCHEMES……xii

Chapter Page

1. INTRODUCTION……1

1.1 Introduction of this study……1

1.2 Importance of solar energy and the history of solar cell technology……4

1.3 Concept of solar cell……6

1.3.1 Definition of solar cell……6

1.3.2 Concept of P-N junction……6

1.3.3 Cell structure……7

1.3.4 Dark current and photocurrent……8

1.3.5 Output characteristics of a solar cell……10

1.3.6 Carriers separation and collection……11

1.4 Important factors for solar cell performance……12

1.4.1 Band gap of materials……12

1.4.2 *Absorption of light* ……13

1.5 Introduction of thin film solar cells……14

1.5.1 Thin film solar cells……14

1.5.2 Requirements of materials for thin film solar cells……15

1.5.3 Applications of thin film technologies……15

1.6 Introduction of ZnO:Al and Cu_2O……..17

1.6.1 Properties of Al doped zinc oxide (ZnO:Al)……..17

1.6.2 Properties of cuprous oxide (Cu_2O)……..……18

1.6.3 Review of major ZnO:Al/Cu_2O heterojunction solar cell studies……19

1.6.3.1 High temperature process of Cu2O/AZO heterojunction solar cell……..……19

1.6.3.2 RF Sputtered Cu_2O/ZnO heterojunction solar cell……..……20

1.6.3.3 Electrochemical deposition Cu2O/ITO heterojunction solar cell……..…22

2. EXPERIMENTS……..……..……..……..…23

2.1 Thin film processes used in this study……..……..……..…23

2.1.1 Sputtering……..23

2.1.2 Chemical bath deposition (CBD)……24

2.1.3 Rapid thermal process (RTP)……..……25

2.2 Fabrication of semi-transparent heterojunctions……26

2.2.1 Preparation of glass substrates……..……26

2.2.2 Sputtered deposition of ITO, AZO and Cu_2O……..…26

2.2.3 Deposition of intrinsic ZnO as a buffer layer in the heterojunction……...27

2.2.3.1 Sputter i-ZnO……..27

2.2.3.2 Chemical bath deposition of i-ZnO……..28

2.3 Morphology and structure for analyses of thin-films……..……28

2.3.1 Scanning Electron Microscope……28

2.3.2 X-ray diffraction (XRD) for structural analysis……...29

2.4 I-V characterization of the heterojunctions……..29

3. RESULTS AND DISCUSSIONS……..……31

3.1 Competitive nucleation rate and the effect of solution pH in CBD of i-ZnO……..31

3.1.1 Effect of substrates……31

3.1.2 Effect of pH value……32

3.1.3 X-ray diffraction analysis on the ZnO thin-films……33

3.1.4 Analysis of Cu_2O annealed using a rapid thermal annealer……34

3.2 Analysis of the heterojunction……35

3.2.1 I-V characteristics……35

3.2.2 Role of the buffer layer: i-ZnO……36

3.2.3 The effect of deposition technologies……37

3.2.4 The effect of i-ZnO thickness……37

3.2.5 The lattice mismatch……38

3.2.6 Performance of cell under light……38

4. CONCLUSION……39

5. FUTURE WORK……40

REFERENCES……41

BIOGRAPHICAL INFORMATION……45

LIST OF ILLUSTRATIONS

Figure Page

1.1 The applications of transparent solar cell, (a) electrical vehicle mounted solar panel on its roof and (b) solar panels are installed on roof of botanical garden……..……..…….……..…1

1.2 LC variable attenuate goggle…….……..……..……..……..……..…3

1.3 Statistics of energy usage in 2010……..……..……4

1.4 Three generations of solar cell technologies: (a) 1st generation (single crystal Silicon); (b) 2nd generation CIGS and (c) 3rd generation (polymer solar cell)…….....……..……..……...5

1.5 The solar cell is the substitution of battery in a circuit……...……6

1.6 Band diagram of (a) n-type and p-type semi-conductor and (b) p-n junction…….……..……..……..…7

1.7 Photogenerated electron-hole pairs are separated by internal electrical field……..……..……..7

1.8 I-V characteristic of ideal diode under light and dark……..……..……9

1.9 When E (photon energy) > E_g (band gap of material), electrons can be excited jumping from a valance band to a conduction band. In contrary, no electron in ground state can be excited to excited state when E < E_g……..……..……..9

1.10 Relationship between GaAs quantum efficiency and solar photon flux density…...……..……10

1.11 The current density (J) – Voltage (V) characteristics of a solar cell. The maximum power density (P_d) is equal to J_mV_m……..……..…….....11

1.12 Effect of (a) increasing series resistance (R_s) and (b) decreasing shunt resistance (R_{sh}) on a solar cell. In the case of $R_s = 0$ and $R_{sh}=\infty$, the out power will be the maximum……..……..……..…12

1.13 The theoretically calculated efficiency as the function of band gap……..……..13

1.14 Increasing of optical path through (a) surface texturing and (b) back side reflector……..……..……14

1.15 The integrated structure of thin film solar cells……..……...15

1.16 The schematic of triple-junction solar cell……..……..…..……..16

1.17 The 18.7% efficiency of CIGS on PI films…….....……..……..17

1.18 Formation energy for major defects in
ZnO at (a) Zn-rich and (b) O-rich……..……..18

1.19 Formation energy comparisons for intrinsic defects in
Cu_2O at the condition of (a) Cu-rich and (b) Cu-poor……..……..……19

1.20 (a) The structure of AZO/ZnO/Cu_2O solar cell.
(b) J-V measurement of AZO/ZnO/Cu_2O with
different deposition temperature……..……..20

1.21 (a) Schematic structure of p-Cu2O/i-ZnO/n-ZnO
solar cell, (b) reaction schemes of CN treatment……..……..……21

1.22 Electrical properties as function of CN treatment time: (a) trap
concentration and (b) carrier concentration……..…..21

1.23 I-V characteristics for Cu_2O/ZnO/ITO heterojunction.
The inset is the structure of the cell……..…….22

2.1 The schematic of a planar diodes sputtering system……..……..……..23

2.2 RF sputtering system used in this study……..……...……24

2.3 The configuration of CBD……..……..……25

2.4 The image of rapid thermal process……..……..……..……26

2.5 Hitachi S-3000N scanning electron
microscope (SEM) at UTA's CCMB……..……..29

2.6 D-500 (Siemens) X-ray Diffractometer……..……..……..……..……29

3.1 The SEM images of film deposited at low pH value on (a) bare glass,
(b) Si wafer and (c) AZO coated glass……..……...……..31

3.2 SEM micrographs of i-ZnO: (a) CBD (pH=8.5) i-ZnO,
(b) CBD (pH=10) i-ZnO, and (c) CBD (pH=10)
i-ZnO with ultrasonication……..……..……..……..……..…32

3.3 XRD obtained from the samples: (a) sputtered AZO,
(b) CBD (pH=8.5) i-ZnO on top of sputtered AZO,
(c) CBD (pH=10) i-ZnO with ultrasonication
on top of sputtered AZO……....……..……..……..……..…34

3.4 SEM images of Cu_2O. (a) as-deposited and
(b) annealed at 350^{o}C for 30 min……..……..……..……..…34

3.5 XRD profiles of Cu2O/sputtered i-ZnO/AZO/glass……..……..…35

3.6 Dark I-V characteristics of AZO/i-ZnO/Cu_2O
heterojunctions with different i-ZnO buffer layer……..……..……..……36

3.7 Carrier transport across junction when the density
of interface defects is (a) low and (b) high…….……..……..……36

3.8 P-N junction at forward bias……..……..……..……37

LIST OF TABLES

Table Page

2.1 Sputter deposition of ITO, AZO and Cu_2O……..……..……..…..27

2.2 Summary of sputtered i-ZnO……...……..……..27

2.3 Variables used for the CBD of i-ZnO……..……..……..…...…28

LIST OF SCHEMES

Scheme Page

3.1 A series of chemical reaction for CBD i-ZnO……..32

CHAPTER 1

INTRODUCTION

1.1 Introduction of this study

Building-integrated photovoltaic is the concept that solar cell modules can replace some building components such as building windows. Nowadays, the solar cell panels are not only the power generators, but also the part of decoration of architecture. It would be beneficial to those components if the structure itself can be multi-functional so it serves as a structure itself, but also a part of energy harvesting. Transparent part of the structure can be either constructed with or supplemented with conducting oxides those can be fabricated into a photovoltaic device. Ultimately, the device needs to be optimized for the amount of light absorption necessary for the power generation and the transparency necessary for structural functionality. For example, the semi-transparent solar cell can be integrated with sun roof of electric automobiles (Fig. 1.1 (a)), so that allowable driving distance of electric vehicle will be enhanced. In addition, the roof of a botanical garden can be also integrated with solar panels (Fig.1.1 (b)); hence, the power consumption of itself can be satisfied without being supported externally.

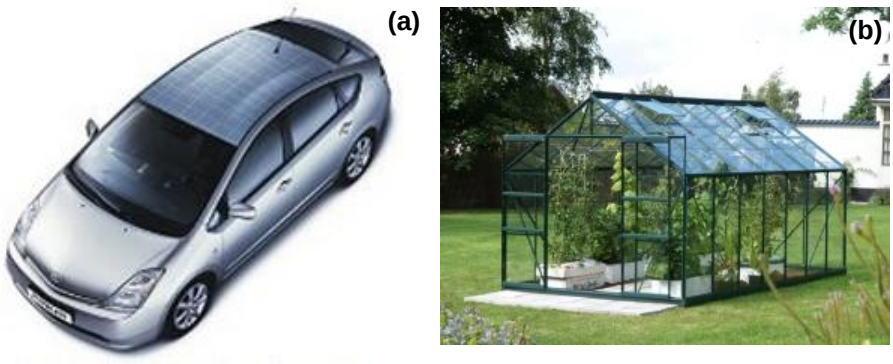

Fig. 1.1 The applications of transparent solar cell, (a) electrical vehicle mounted solar panel on its roof [1] and (b) solar panels are installed on roof of botanical garden [2].

The organic based solar cell has very high potential satisfying the demand of semi-transparent applications. It possesses the capable of mechanical flexibility and low manufacturing cost, which is superior to traditional inorganic based solar cells. In 2011, Massachusetts Institute of Technology successfully fabricated a transparent organic solar cell on glass with 2.4% efficiency and over 55% transmittance in visible light spectrum [4]. However, the organic solar cells still has several drawbacks to be solved including degradation issue due to air exposure.

Among other different type of semi-transparent applications, Cu_2O/ZnO:Al (AZO) heterojunction solar cell has caught much attention recently. The natural p-type Cu_2O has band gap of 2.2 eV, which stands at the balance between transmittance and absorption. The high minority carrier diffusion length is also expected for Cu_2O. At the same time, the n-type Transparent Conducting Oxide (TCO) AZO is a well-developed window layer for solar cell applications. It is expected to have good transmittance at the visible light spectrum due to its high band gap of 3.2 eV. The best power conversion efficiency (PCE) of about 4% was recently achieved for Cu_2O/AZO heterojunction solar cell [5]. In that study, high quality of Cu_2O was fabricated by oxidizing Cu foil at over 1000^oC. Nevertheless, the high process temperature limits the capability of applications because it is not feasible fabricating devices on polymer-based flexible applications. In order to circumvent the disadvantage, the low-temperature thin-film deposition was also employed to fabricate the heterojunctions. While p-Cu_2O/n-AZO cell was fabricated by RF magnetron sputtering, extra substrate heating was applied [6]. Nevertheless, the efficiency of the device was only around 0.7%. In another study, electrochemical deposition as a low-temperature process was introduced to fabricate Cu_2O/ITO heterojunction Cu_2O/ITO heterojunction [7]. However, the photovoltage of device under light is scanty.

The goal of this study is to fabricate working Cu_2O/AZO semi-transparent solar cells at room temperature. Hence, the device can be applied on various substrates including polymer substrates. Although the efficiency of room temperature processed device will be low as

expected due to the property of low temperature deposited Cu_2O, the device still can be enough for some voltage-driven applications, such as, liquid crystal (LC) variable attenuator goggle (Fig. 1.2). The most importantly, it will stand on vantage point if the devices can be fabricated at low temperature.

Fig. 1.2 LC variable attenuate goggle [3].

In order to realize the device at room temperature, AZO/Cu_2O heterojunction was realized by an RF sputter without any thermal treatment in this study. The short minority carrier diffusion length of as-deposited Cu_2O can be overcome by utilizing thinner Cu_2O. Additionally, the usage of a buffer layer in the junction structure is studied in this work. Generally believing is that the plasma damage from the subsequent sputtering process creates high density of defects at the interface. Hence, recombination will be severe at the high defects density junction interface. In addition, the type of buffer layer and method of fabrication play an important role in improving the performance of the thin film solar cells which was reported by many other groups [8]. For instance, CdS deposited by chemical bath deposition (CBD) has been demonstrated as the best buffer layer for Cu(In,Ga)Se_2 (CIGS) thin film solar cells [9]. In fact, the positive benefit of i-ZnO buffer to devices has been previously shown, but without much explanation [10]. Therefore, chemical bath deposition (CBD) has been used depositing intrinsic ZnO (i-ZnO) buffer layer in the junction in order to completely remove plasma damage, and sputtered i-ZnO has been fabricated as comparison. In this thesis, the effect of i-ZnO buffer layer on AZO prior to the sputter deposition of Cu_2O and show its effect on the performance of the heterojunction solar cell.

1.2 Importance of solar energy and the history of solar cell technology

Energy crisis is not just a topic. It is something that we are encountering seriously right now. We have used oil, gas or coal as our energy sources for several centuries already, and those natural sources are going to be out in the near future. It is hard to imagine that the life of human being without nuclear, gasoline and coal. Certainly, our advanced technologies are going to be disappeared. In addition, severe climate change due to greenhouse effect is imminent. Over 60% of greenhouse effect could be attributed to the production of CO_2, which is from the consumption of hydrocarbon fuel [11]. As of now, people are aware of crisis to the shortage of non-reproducible energy sources. All the countries are looking for other energy sources instead of non-reproducible energy. On 2010, the overall energy statistics of world from International Energy Agency (IEA) indicated that the usage of solar energy is less than 1% of total energy as Fig. 1.3 [12]. .Among the all different the sorts of renewable energy sources, the solar energy has caught so much attention recently although popularization of solar power

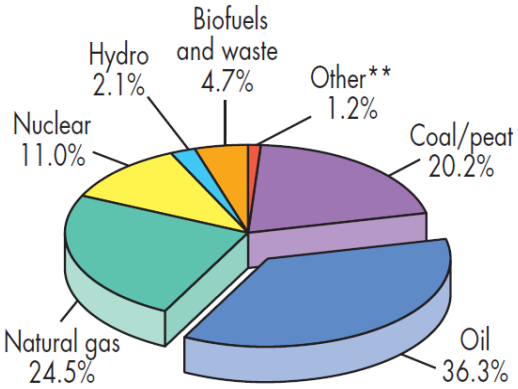

Fig. 1.3 Statistics of energy usage on 2010 [12]

usage is still low. Solar energy technology is definitely one of the most attractive alternative energy sources in the future. It has the properties of non-limited, non-polluted, and easy to being utilize. ‘The solar radiation reaching the earth‘s surface in one year provides more than 10,000 times the world‘s yearly energy needs’ [13, p.1]. Therefore, solar energy is going to be the hope to human’s future.

Photovoltaic (PV) phenomena were first discovered by Alexandre-Edmon Becquerel, a French physicist, in 1839. Since then, the solar cells became a part of energy producer. The PV devices separate light induced carriers (electrons and holes), and extract them generating electricity. The solar cell could be divided into three categories as following according to different fabrication technologies.

1st generation: single crystal silicon (Fig. 1.4 (a))

2nd generation: amorphous silicon, polycrystalline silicon, cadmium telluride, $Cu(In,Ga)Se_2$ (CIGS) (Fig. 1.4 (b)).

3rd generation: organic solar cells (Fig. 1.4 (c)), nanocrystal solar cells, and dye sensitized solar cells.

First generation solar cell is still dominating market, which is about 86% of total solar cell market. This type of cell is made of p-type silicon wafer and an extremely thin n-type emitter. The advantages of first generation cell are (i): high efficiency: the recent reported PCE for crystalline Si cell is 25% [14], and (ii) the mature fabrication process: The fabrication processes of Si wafers are well established in semiconductor industry for several decades already. However, many disadvantages of first generation cells are including high cost of manufacturing process and low absorption of high energy photons due to low band gap of silicon (1.1 eV). Hence, thin film solar cells to overcome the challenges Si technology faces. The main advantages of thin film solar cells and third generation solar cell include that the fabrication cost

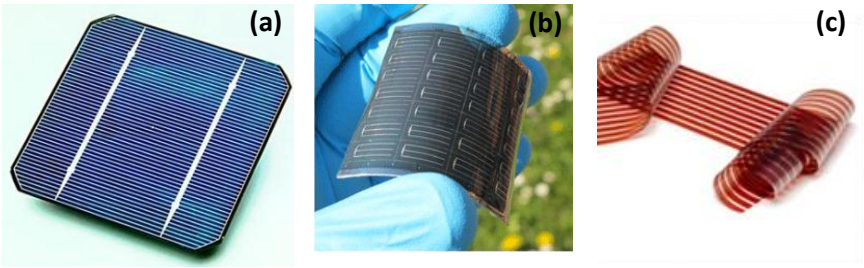

Fig. 1.4 Three generations of solar cell technologies: (a) 1st generation (single crystal Silicon) [15]; (b) 2nd generation CIGS [16] and (c) 3rd generation (polymer solar cell) [17].

is reduced dramatically compared to the first generation cells, and that the monolithic integration of the cells into high power module is also achievable.

In my study, thin film heterojunction solar cell offers those possibilities. Transparency is achievable through high band gap materials, and integrated structure is also realized by Transparent Conducting Oxide (TCO). The detail will be discussed succeedingly.

1.3 Concept of solar cell

1.3.1 Definition of solar cell

The simplest concept of solar cell is that the solar cell is substitution of battery when solar cell is operating under light (Fig.1.5) [18]. The open circuit voltage (V_{OC}) is at zero current. On the other hand, the short circuit current (I_{SC}) is when the cell without any load under light. If the load is presented in the circuit, the relation of voltage (V), current (I), and resistance (R) of load will follow ohm's law (V=IR). In other words, I and V will vary as function of light intensity and load.

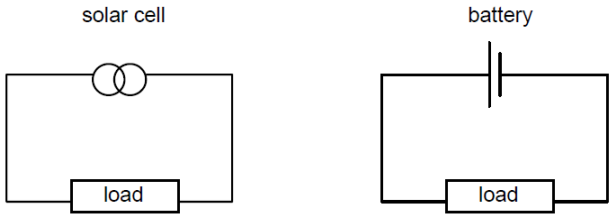

Fig. 1.5 The solar cell is the substitution of battery in a circuit [18].

1.3.2 Concept of P-N junction

Solar cells have ability to separate photogenerated electrons and holes generating electricity. The solar cell is one of the P-N junction applications. P-N junction consists of p-type and n-type materials, which have different types of dopants. P-type material has larger work function (Φ_p) than that of n-type (Φ_n) material as shown in Fig. 1.6 (b). Fermi-level (E_F), which is the function of dopant concentration (Fig. 1.6 (a)), will line up under equilibrium when two

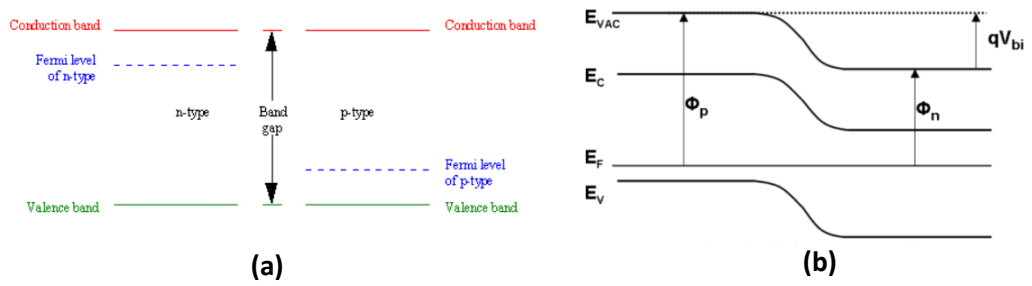

Fig. 1.6 Band diagram of (a) n-type and p-type semi-conductor [19] and (b) p-n junction [18].

materials are in contact as shown in Fig. 1.6 (b). Under equilibrium, the internal built-in electric field will be formed at the junction. The internal electrical field will drag photogenerated electrons from p side to n side (Fig. 1.7), and photogenerated holes will move through opposite direction. In the other words, p-n junction simply separates electrons and holes, and allows them to be collected by electrodes.

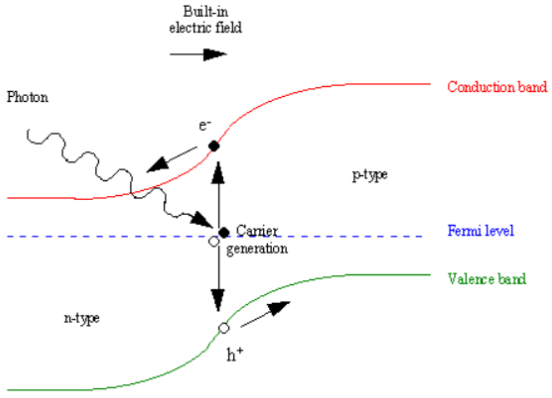

Fig. 1.7 Photogenerated electron-hole pairs are separated by internal electrical field [19].

1.3.3 Cell structures

Homojunction cells are made of one material with different dopant species. The single material can be doped differently on both side of material. The advantage of homojunction is that lattice mismatch will be eliminated since the junction is made of one material. In this

condition, the defects states at the interface will be minimal. Therefore, the recombination at the interface, which is one of the biggest obstacles for collecting electrons and holes can be minor accordingly. Hence, efficiency of cell is expected to be high. However, some materials are intrinsically n-type or p-type due to the low formation energy and ionization energies of the intrinsic defects, and thus cannot be extrinsically doped. Hence, the heterojunction is introduced. It consists of two different materials. The lattice mismatch at the interface is expected higher than homojunction causing high density of defects. Nevertheless, people still often utilize heterojunction structure for solar cell applications on account of the feasibility of dopant. Hence, heterojunction are more suitable than that of homojunction for diode applications sometimes.

In my work, heterojunction structure is applied. The absorber: Cu_2O and window layer: AZO are P- and N- type respectively. Especially for Cu_2O, a natural p-type material, the intrinsic copper vacancies in Cu_2O make it p-type, so creating n-type Cu_2O is not simple task. Although p-type dopant is available for ZnO, ZnO homojunction is still not the option. The reason is bandgap of ZnO is around 3.2 eV, which has low absorption. The efficiency of ZnO homojunction is obviously believed to be low.

1.3.4 Dark current and photocurrent

As I mentioned in previous section, P-N junction possesses potential discrepancy between n-type and p-type. The concept of dark current is that the current is induced by internal electrical field under dark, which is originated from existed of the electrons and holes. In the photovoltaic device, the dark current can be also defined as induced current under reversed bias. The I-V characteristics of photovoltaic device will most likely to have rectification behavior under dark as Fig. 1.8. Dark current increases rapidly under forward bias, and is almost constant under reverse bias. This solar cell typically has this asymmetric rectifying characteristic in order to efficiently separate electrons and holes under light. The dark current density (J_0) of an ideal diode can be described as eq. 1.1

$$J_{dark}(V) = J_0 (e^{eV/kBT}-1) \qquad \text{(eq. 1.1)}$$

J_0 is saturated current, k_BT is thermal energy [18].

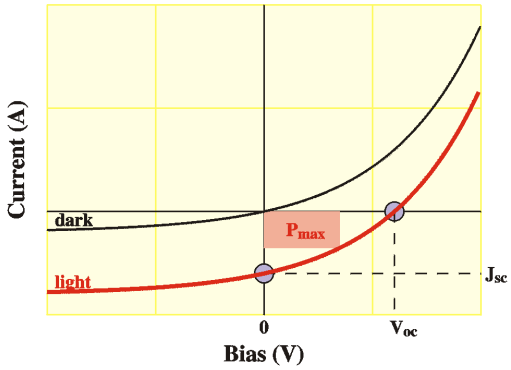

Fig. 1.8 I-V characteristic of ideal diode under light and dark [20].

Photocurrent, it is the current induced under light. It is dependent of light intensity flux and quantum efficiency (QE). Basically, the energy of incident photons is larger than band gap of absorber, the electrons at valance band will be excited to conduction band as shown in Fig 1.9. In fact, the incident light flux and energy of photons have been the key factor determining the photo generated current. The QE(E) is the likelihood of incoming photons with energy E can excite an electron to be collected. The photocurrent, which is equal to J_{SC} is described as eq. 1.2.

$$J_{SC} = e \int b_s(E)\, QE(E)\, dE \qquad \text{(eq. 1.2)}$$

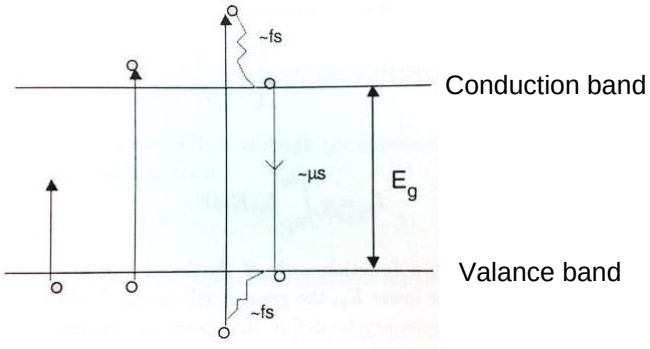

Fig. 1.9 When E (incident photon energy) > E_g (band gap of material), electrons can be excited jumping from a valance band to a conduction band. In contrary, no electron in ground state can be excited to excited state when $E < E_g$ [18].

where e is an electron charge, $b_s(E)$ is the flux density of incoming light, and QE is the function of material's absorption coefficient and QE can accurately present the spectroscopic performance of a solar cell [18]. Fig. 1.10 shows an example of the relationship between QE of a GaAs cell and the solar spectrum. In this case, we may anticipate that the GaAs solar cell will have high efficiency because it has high QE within spectrum range where high photon flux density is.

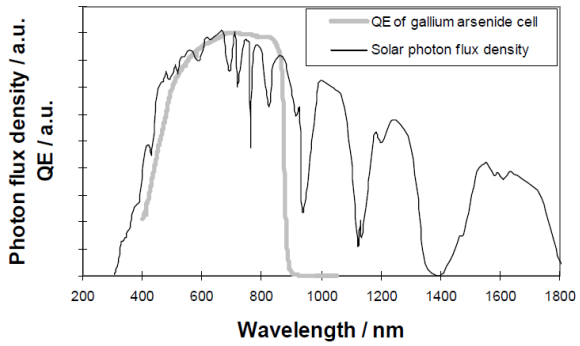

Fig. 1.10 Relationship between GaAs quantum efficiency and solar photon flux density [18].

Therefore, the total current density (J) of ideal diode will be presented as eq. 1.3 [18]

$$J = J_{SC} - J_{dark}(V) = J_{SC} - J_0 \left(e^{eV/KBT}-1\right) \qquad \text{(eq. 1.3)}$$

In the case of non-ideal diode behavior, the eq. 1.3 will become eq. 1.4

$$J = J_{SC} - J_{dark}(V) = J_{SC} - J_0 \left(e^{eV/nKBT}-1\right) \qquad \text{(eq. 1.4)}$$

where n is ideality factor, and equal to 1 for an ideal diode [18]. For a non-ideal diode, which is typical for real devices, n may be larger than 1. For some of the heterojunction solar cell, value of n could be over two due to the tunneling effect when potential barrier gets smaller under illumination. In other words, electrons can tunnel through junction without climbing barrier.

1.3.5 Output characteristics of a solar cell

The power density of solar cell is written as eq. 1.5 [18].

$$P_d = J\,V \qquad \text{(eq.1.5)}$$

The P_d is maximum when the voltage is V_m, and current is J_m as shown in Fig. 1.11. Therefore, the maximum power will be reached when the resistance of load is at the optimized value through to ohm's law. The fill factor (FF), the parameter could represent the squareness of the I-V curve, is given by eq. 1.6.

$$FF = J_m V_m / J_{SC} V_{OC} \qquad \text{(eq. 1.6)}$$

Generally, FF is within the range of 0.25 to1. In addition, the most important parameter which represents the quality of solar cell is the power conversion efficiency (Ƞ). It will be the ratio of maximum power density to total incoming light power density (P_s), which is shown as eq. 1.7.

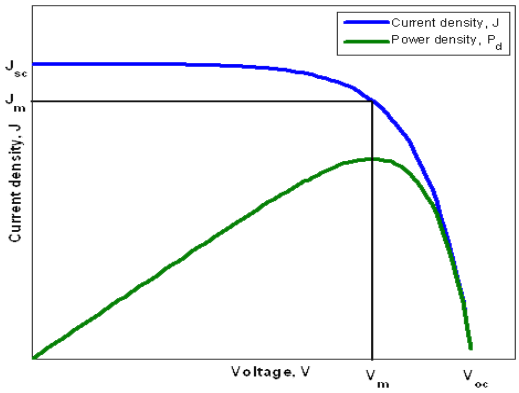

Fig. 1.11 The current density (J) – Voltage (V) characteristics of a solar cell. The maximum power density (P_d) is equal to $J_m V_m$ [21].

$$Ƞ = J_m V_m / P_s \qquad \text{(eq. 1.7)}$$

The four parameters (Ƞ, J_{SC}, V_{OC}, and FF) characterize the performance of a solar cell. J_{SC} is inversely proportional to V_{OC}. Fundamentally, J_{SC} and V_{OC} are associated with the materials' band-gap.

1.3.6 Carriers separation and collection

It is important to understand how well the P-N junction can separate the electron-hole pair when they are generated by incident photons. This is based on internal electrical field, which is originated from work function of materials. Besides, low energy loss is another important factor. The carriers have to be able get to external electrical circuit before they meet each other and recombine. The obstacle of carrier transportation could be the presence of

defects in the medium. Those defects can provide the state for recombination. Also, high resistance of material can absorb the energy of electrons while they are moving around, in other

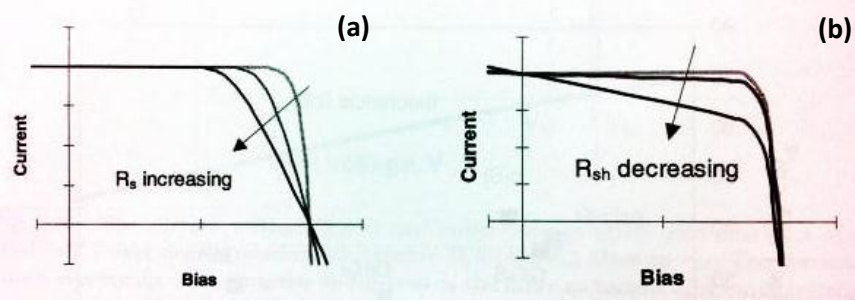

Fig. 1.12 Effect of (a) increasing series resistance (R_s) and (b) decreasing shunt resistance (R_{sh}) on a solar cell. In the case of $R_s = 0$ and $R_{sh}=\infty$, the out power will be the maximum [18].

words, the energy of carriers will be eliminated. The reversed current leakage between n- and p-type is also an issue for degrading performance of solar cell. Shunt resistance should be as high as possible in order to prevent vertically reversed current against photogenerated current. Therefore, the good candidate for solar cell applications should be low in series resistance, but high in shunt resistance as shown in Fig. 1.12 [18].

1.4 Important factors for solar cell performance

1.4.1 Band gap of materials

Two parameters determine the solar cell efficiency (Ƞ) - one is band gap (E_g) and the other is incident light flux as explained previously. This section is going to mainly focusing on effect of E_g. When we assume the incoming light flux is fixed, so that the Ƞ will be determined by E_g [22]. For an absorber with a large band gap, many incident photons pass the absorber through without being absorbed due to their insufficient energy. In this case, photocurrent of the device will be very small. On the other hand, the photovoltage becomes low if the band gap of the absorber is very small. Hence, the choice of the band gap should be first priority while engineers are designing photovoltaic devices. Fig. 1.13 shows calculated value of efficiency

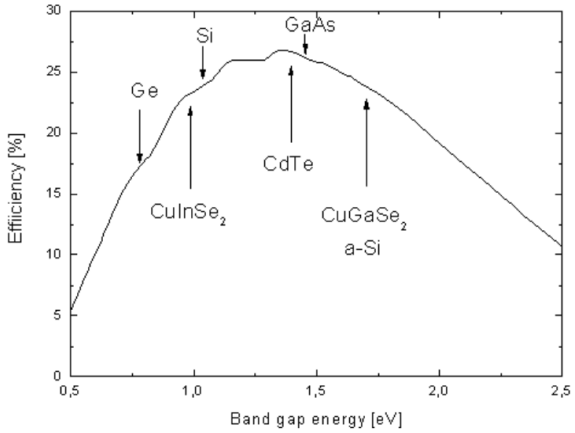

Fig. 1.13 The theoretically calculated efficiency as the function of band gap [22].

versus band gap. It is important to point out that the preference of materials is much relied on the function of applications. In my case, semi-transparent solar cell has to be transparent. Therefore, the bottom line is that we have to utilize materials with higher band gap, such as, Cu_2O. Therefore, the efficiency of cell will be foreseeably worse than non-transparent solar cell.

1.4.2 Absorption of light

While high absorption coefficient of materials is always desired for solar cell applications, enhancing absorption by increasing optical path in the materials can be attempted, so that the absorption will be enhanced accordingly. One method is to randomize surface of the cell. As Fig. 1.14 (a) shown, randomized texturing surface will efficiently provide more chance to confine the light within materials. Furthermore, back side reflector (Fig. 1.14(b)) has been used as well [19]. The optical path can be enhanced significantly via these two strategies. In fact, the simplest way to increase the optical path is to increase the thickness of absorber as much as possible. However, managing thickness of absorber is not trivial because the diffusion length of minority carriers needs to be concerned as well. If the diffusion length of minority carriers is short, then thicker films contrarily make the performance of cell worse. For typical crystalline Si cells, the absorber is usually around a few hundred μm thick.

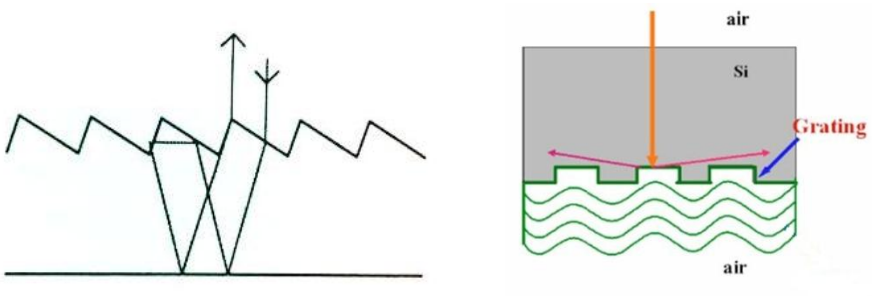

Fig. 1.14 Increasing of optical path through (a) surface texturing [18] and (b) back side reflector [23].

1.5 Introduction of thin film solar cells

1.5.1 Thin film solar cells

In order to overcome some of the drawbacks of first generation cell, such as, high cost of fabrication process, and incapability of absorbing the energy above the blue and violet spectrum, the thin film solar cells has been good substituted candidates of first generation cells, silicon wafer based solar cell. Unlike first generation cells, thin film solar cell has some of the advantages which are superior to first generation cells. Firstly, thin film solar cell can dramatically reduce the usage of materials, which can drastically solve issue of silicon shortage when it happens. Secondly, thin film solar cell has comparably cheaper processing costs than first generation cells. The 50% of whole module fabricating cost of silicon based solar cell is occupied by silicon wafers [24]. The cost of manufacturing device could be reduced by replacing silicon wafer to alternative thin films. Lowering prime cost is very important concern for the commercial products. Thirdly, the monolithic integration of cells into a module is achievable as shown in Fig. 1.15. The configuration of thin film solar will significantly reduce the weight of product, and improve the sustainability of product at the windy area, for example.

Finally, thin films give engineers more possibilities of designing devices. People can deposit any material on any different substrates. In addition to that, the high efficiency multi-junction cells were also realized by thin film technologies, which can overcome losing

absorption for either high or low wavelength of light. From all above, thin film solar cell has potential to revolutionarily replace first generation solar cells.

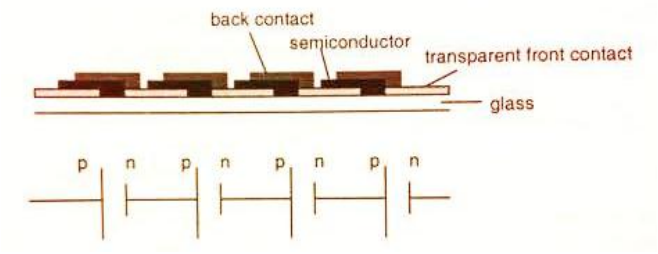

Fig. 1.15 The integrated structure of thin film solar cells [18].

1.5.2 Requirements of materials for thin film solar cells

As mentioned formally, thin film solar cell materials possess superiority over first generation solar cells. The thin film materials have to be abundant, low fabricating cost, and non-toxic. They should have better absorption than silicon. In this conception, the thickness of device can be reduced, and possibly shorter diffusion length can be tolerated. Also, purity of film can be compromised. The most importantly, the materials need to be doped headily. Furthermore, the stability of materials is another crucial factor. For example, amorphous silicon (a-Si), one of the thin-film photovoltaic materials, has light degradation issue due to Staebler-Wronski effect, which is the number of dangling bonds will increase with light exposure [25].

1.5.3 Applications of thin film technologies

World's highest efficiency triple-junction solar cell

As mentioned at 1.4.2, the thickness of film can be reduced when the absorption of film is higher in any ways. The multi-junction solar cell is the product which is practically pushed to the limit of thin film technologies. Basically, it consists of a few different band gaps of materials as its absorber, so that the wider spectrum of the light could be absorbed. Although it still has its drawbacks, such as lattices mismatch and current matching issues, the record efficiency of the multi-junction cell stunned the world. In 2010, the highest efficiency of multi-junction cell has been revealed in Japan. It Is an InGaP/GaAs/InGaAs triple-junction solar cell. The efficiency

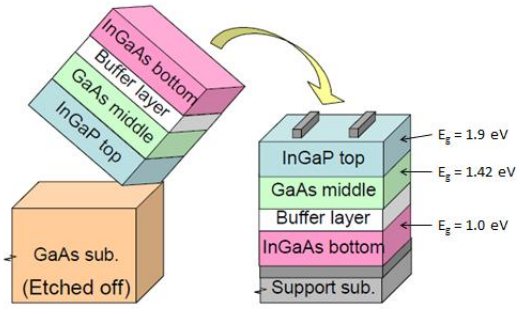

Fig. 1.16 The schematic of triple-junction solar cell [26].

has been reached 35.8% [26]. The device was first grown on GaAs substrates by metal organic chemical vapor deposition method, and then the stack of layer was flipped over as explained in Fig. 1.16. In this paper, the lattice-mismatching was reduced by 1% of indium doping, which eliminated the presence of dislocations at the interface. Additionally, the current matching has been achieved by replacing typical Ge (Eg=0.6eV) bottom junction to InGaAs (Eg=1eV) junction. V_{OC} was as high as 3.0 volts.

In short, 35% efficiency or higher, which beats 25% of crystalline Si solar cell, is achievable through thin film technologies.

Polycrystalline CIGS solar cells on flexible substrates

The flexible capability is another important merit of thin films technologies. One of the next generation thin film solar cell materials is polycrystalline chalcopyrite, CIGS. People have demonstrated over 20% efficient CIGS solar cell on the glass substrates [27]. Recently, the efficiency of CIGS solar cell has reached 18.7% on flexible substrates, polyimide (PI) films [28]. The obstacle was that polymer substrates cannot sustain a process temperature exceeding 500°C, which is usually required for fabricating high efficiency solar cells on glass. Previously, people used to fabricate thin film solar cell on thin glass or metal foil in order to satisfy high temperature process. Fig. 1.16 shows the CIGS cell on PI film. Fig. 1.17 shows the real device of CIGS cell on PI film. Furthermore, the roll-to-roll process becomes feasible once device can

be successfully fabricated on those flexible substrates. The roll-to-roll process will dramatically enhance manufacture throughput. This makes huge impact to industry when it becomes commercially available.

In short, thin film solar cell can break some of the limitations of Si wafer based solar cell. It has prospective of commercial feasibility. Hence, it definitely has the potential to be one of the next dominated technologies in solar cell field.

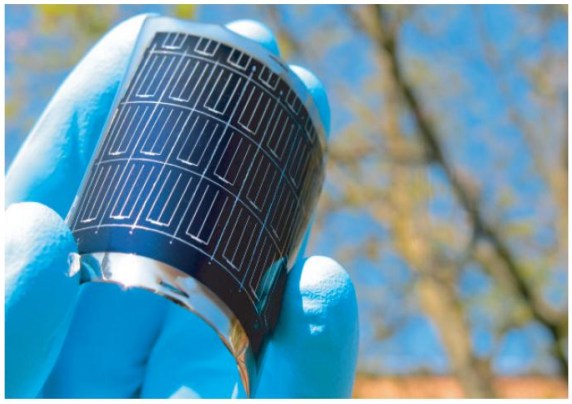

Fig. 1.17 The 18.7% efficiency of CIGS on PI films [28].

1.6 Introduction of ZnO:Al and Cu_2O

1.6.1 Properties of Al doped zinc oxide (ZnO: Al)

The n-type ZnO: Al (AZO) has been used as a window layer in various thin-film solar cell applications because of its high band-gap, which is about 3.3 eV and consequent transparency in visible wavelength range [29-b]. Those properties make AZO suitable to semi-transparent solar cell, the targeted study in this project. In addition, AZO is a stable compound, and will not likely react with other materials. Most importantly, ZnO is an intrinsically n-type semiconductor due to the existence of oxygen vacancies (V_O) and Zn vacancies (V_{Zn}) [30]. Fig. 1.18 shows the formation energy of various intrinsic defects in ZnO. In the Zn-rich condition, V_O has become dominated defects due to its lowest formation energy (Fig. 1.18 (a)). V_O is like a defect as an electron, and it will increase Fermi-level. For the case of O-rich, V_{Zn} become major

defects because it has the lowest formation energy than other defects as shown Fig. 1.18 (b). V_{Zn} has -2 charge, so that it makes ZnO as n-type [30].

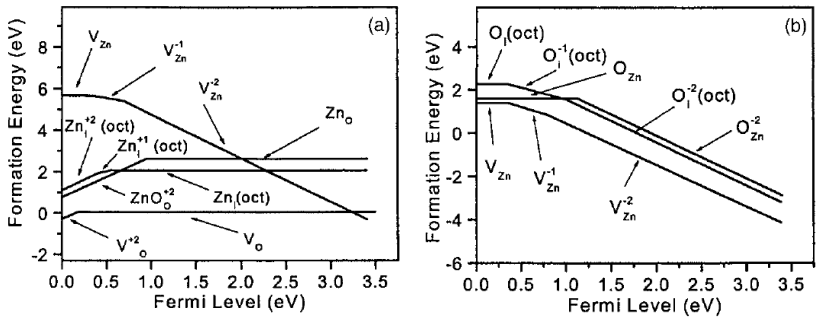

Fig. 1.18 Formation energy for major defects in ZnO at (a) Zn-rich and (b) O-rich [30].

For n-type doping, group III and group VII can be an extrinsic dopant for ZnO, and has been done by other groups [31]. Al is one of the common n-type dopants for ZnO and it substitutes Zn. Many groups have fabricated high conductivity AZO via many different technologies, such as, pulsed laser deposition (PLD) [32], chemical-vapor deposition [33], and sputtering [34]. The resistivity of AZO can reach as low as 1.2 X 10^{-4} Ω cm [35].

1.6.2 Properties of cuprous oxide (Cu_2O)

The transparent conducting Cu_2O has potential to be a semi-transparent absorber because of its direct bandgap of about 2.2 eV and high absorption coefficient [36]. The several advantages of Cu_2O including non-toxic materials, plentiful source of copper, and low cost of production. The Cu_2O, is also expected to show a higher carrier mobility and a longer minority carrier diffusion length than most metallic oxides because the energy level of the fully filled *d*-orbital of copper cation is close to *2p*-orbital of oxygen anion often allows sizeable covalency in the bonding between them forming a substantially delocalized valence band edge [37]. In addition, the low formation and ionization energies of some of the intrinsic defects make Cu_2O as an intrinsically p-type semiconductor. In fact, the copper vacancy (V_{Cu}) in Cu_2O has the lowest formation energy among other intrinsic defects in Cu_2O, such as, oxygen vacancy (V_O), oxygen interstitial (O_i) and copper interstitial (Cu_i). Fig. 1.18 shows the theoretically calculated

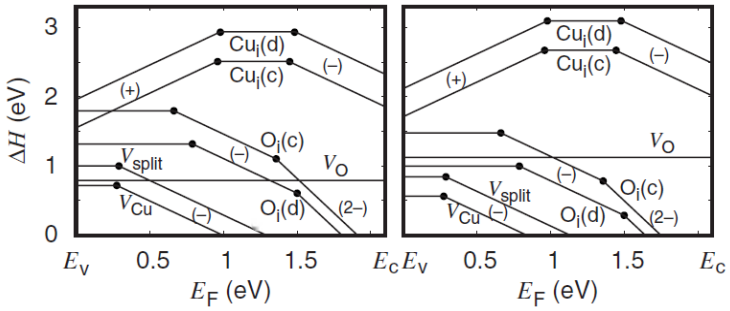

Fig. 1.19 Formation energy comparisons for intrinsic defects in Cu_2O at the condition of (a) Cu-rich and (b) Cu-poor. [38]

formation energy of different intrinsic defects in Cu_2O [38]. V_{Cu} possesses overall the lowest formation energy regardless of Cu-poor or Cu-rich condition. In addition, various technologies had been utilized fabricating Cu_2O heterojunction including thermal oxidation [5], electrochemical deposition [39], and PLD [5]. For thermal oxidation method, oxidation of a high quality Cu sheet was performed at 1000 °C. Those make the processes complex, and bring up the cost. Besides, the major problem of Cu_2O made by electrochemical deposition is high resistivity, when compare to thermal oxidation process. In short, most Cu_2O fabrication processes either required a high-temperature thermal treatment or resulted in Cu_2O with poor electrical properties.

1.6.3 Review of major ZnO:Al/Cu_2O heterojunction solar cell studies

1.6.3.1 High temperature process of Cu_2O/AZO heterojunction solar cell

The highest PCE reported so far for the AZO/Cu_2O thin-film heterojunction solar cell was achieved most recently in 2011, which is about 4% [5]. In this particular study, the p-type absorber Cu_2O was made by oxidizing Cu foil at very high temperature over 1000 °C in order to obtain high quality of Cu_2O. ZnO and AZO were deposited by PLD at subsequent processes. Fig. 1.20 (a) shows structure of the n^+-AZO/n-ZnO/p-Cu_2O heterojunction solar cell.

In this paper, they claimed that the presence of n-ZnO film helps reducing damage on the surface of Cu_2O from subsequent process, so that the defects on Cu_2O surface have been reduced. However, the performance of cell decreases once the thickness of ZnO over 50nm. This is attributed to short minority carrier diffusion length in ZnO, in other words, the defects were increased as the thickness of ZnO increases. The J-V characteristics of cells have been shown as Fig. 1.20 (b). The ZnO and AZO films deposited under room temperature revealed best cell efficiency which is about 4%. On the other hand, higher temperature process results in lower cell performance. The reason is that carrier concentration of n-type ZnO decreases as temperature increases.

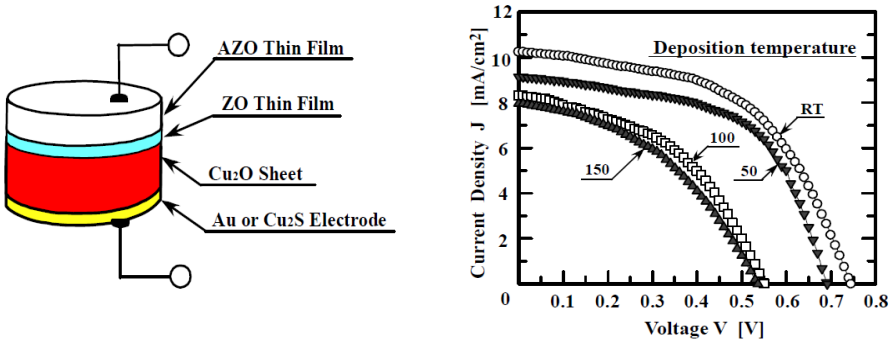

Fig. 1.20 (a) The structure of AZO/ZnO/Cu_2O solar cell. (b) J-V measurement of AZO/ZnO/Cu_2O with different deposition temperature [5].

In short, high efficiency of ZnO/Cu_2O heterojunction solar cell has been realized by thermal oxidation process. Nevertheless, Cu sheet oxidation process limits the diversity of applications. It cannot be applied on transparent applications.

1.6.3.2 RF Sputtered Cu_2O/ZnO heterojunction solar cell

In another study, the heterojunction Cu2O/ZnO (Fig. 1.21 (a)) was fabricated by RF magnetron sputtering with 400^{o}C substrate temperature [6]. They mainly claimed that the defects in the Cu_2O will be the major source of poor cell performance. They were performing the post-deposition crown-ether cyanide (CN) treatment in order to passivate the deep-level defects in the Cu_2O, and the effect of CN treatment was proven by deep level transient spectroscopy.

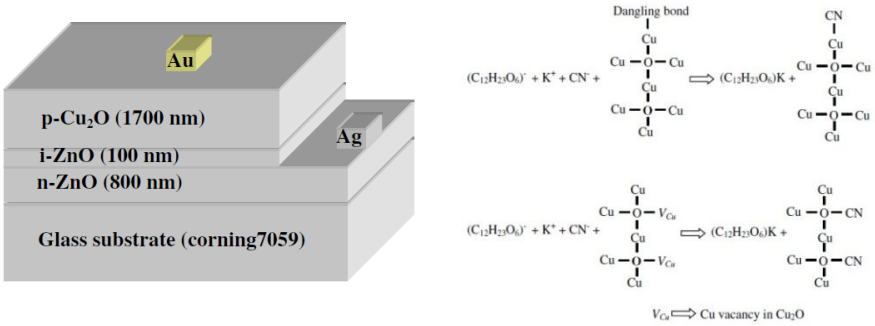

Fig. 1.21 (a) Schematic structure of p-Cu2O/i-ZnO/n-ZnO solar cell, (b) reaction schemes of CN treatment. [6]

The CN treatment was basically preparing KCN solution of xylene containing crown-ether, and the whole device was immersed into the solution for certain period of time. The Fig. 1.21 (b) illustrated the reaction schemes. CN^- ions passivate dangling bonds and copper vacancies in Cu_2O. Copper dangling bonds are donor defects. Therefore, the trap concentration is decreased and holes concentration was increased reasonably as CN treatment time was extended as shown in Fig. 1.22. The I-V characteristic (not shown) had revealed the improvement in efficiency from 0.4% to 0.7% by performing of CN treatment.

In short, substrate heating during the sputtering process and post CN treatment showed the improvement on the quality of Cu_2O. However, the efficiency of cell was still low.

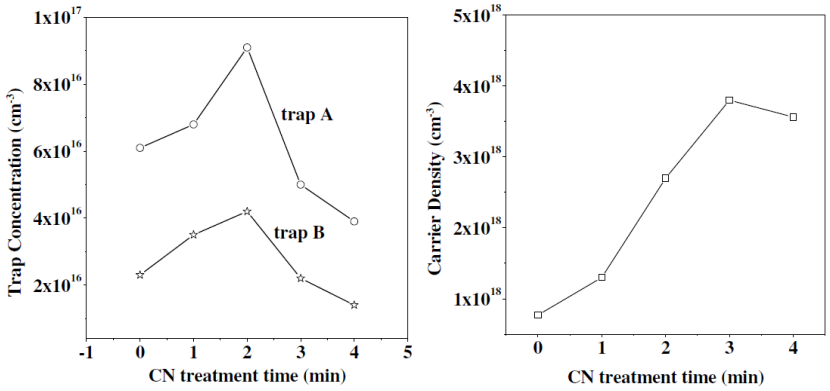

Fig. 1.22 electrical properties as function of CN treatment time: (a) trap concentration and (b) carrier concentration. [6]

1.6.3.3 Electrochemical deposition Cu2O/ITO heterojunction solar cell

This Cu_2O/ITO heterojunction cell was fabricated by electrode deposition method [7]. They claimed that the defects at the interface of Cu_2O and ZnO are significant due to the high lattice mismatch, which will be the recombination center for photogenerated electrons and holes. I-V measurement (Fig. 1.23) was shown that the threshold voltage of cell was about 0.5 volts, which is smaller than theoretically potential barrier between Cu_2O and ITO. It is also the evidence that the presence of defects at the interface.

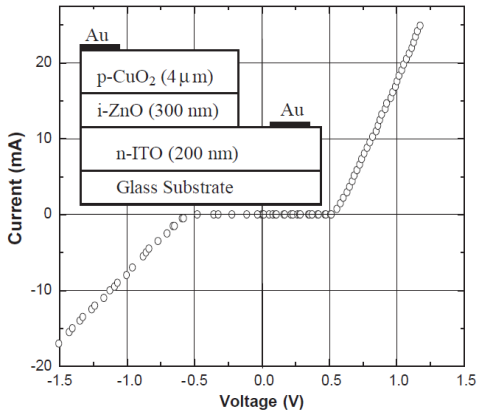

Fig. 1.23 I-V characteristics for Cu_2O/ZnO/ITO heterojunction. The inset is the structure of the cell [7].

In short, the heterojunction of n-ITO/Cu_2O was fabricated through electrochemical deposition method. The problem for this particular case is lack of photocurrent, which could attribute to significant presence of defects at interface or bulk. Furthermore, the short minority carrier diffusion length in Cu_2O could cause poor cell performance under light as well.

CHAPTER 2

EXPERIMENTS

2.1 Thin film processes used in this study

2.1.1 Sputtering

Sputtering is one of the vacuum-based thin-film deposition processes. It is available with two different power sources, which are DC and RF power, and the usage of power is normally depending on the applications. DC power is utilized for conductor, on the other hand, RF power is most likely be used for non-conducting materials in order to prevent arcing issue during process. Arcing is originated from accumulated charges on the targets, and results in degraded deposited thin films. It usually causes increment of defects on the deposited thin films. The sputter system is versatile in terms of sputtering materials when compare to other thin film fabrication technologies, such as, thermal or chemical processes. Almost all materials can be deposited by a sputtering system.

The schematic of sputtering system is shown in Fig. 2.1. The inert carrier gas is always flow during process in order to be ignited as plasma as well as prevent chemical reaction between substrate and target. For the sputtering process, the carrier gas is ionized to plasma state at the beginning of the process. While bias is applied to target, high energy plasma ions

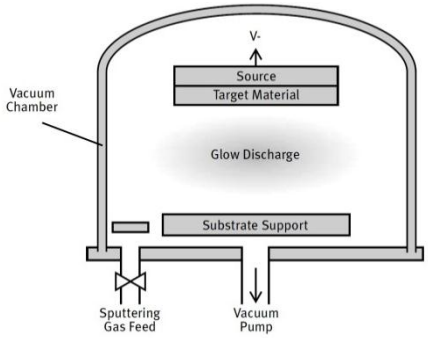

Fig. 2.1 The schematic of a planar diodes sputtering system [40].

strike target. Hence, the target material is sputtered off by ionized gas, and then the material is deposited on the substrate. The base pressure is typically around 10^{-4}~10^{-8} torr range which is depending on desired quality of films. There are several distinct configurations including traditional planar diodes, triode, and magnetron based. The planar diodes types are widely used for long time, and triode types are utilized to obtain thicker film. The planar diodes are recently replaced by magnetron type configuration. The magnetron sputtering system can deposit films with comparably faster deposition rate and wider deposition area compared to traditional planar diodes system. The sputtering system (DMS) used in this study is shown in Fig. 2.2. The sputtering system consists of three target slots allowing the deposition of three different materials in a sequential process without exposing the sample to atmosphere.

Fig. 2.2 RF sputtering system used in this study.

2.1.2 Chemical bath deposition (CBD)

In CBD, a substrate is placed inside an aqueous solution, and the film is grown on the surface of the substrate through chemical reactions. The factors including pH of the solution, type of the substrate, temperature of the bath, position of the substrate, and the speed of stirring could impact the results. The CBD has the advantages of lower cost, and capable for thicker film deposition. As mentioned previously, the best efficiency of CIGS thin film solar cell was achieved by implementing CBD-deposited CdS as its buffer layer [9]. The general belief is that the CBD process has dramatically reduced damage to the film underneath compared to other

vacuum deposition processes. Hence, CBD is commonly used to deposit buffer layers for photovoltaic applications since photogenerated carriers are extremely sensitive to the presence of defects at the interface. Furthermore, CBD is an economical solution process, which is very simple. Fig. 2.3 shows the configuration of CBD. The ultrasonication was employed into CBD in this study to reduce the adhesion of byproduct particles.

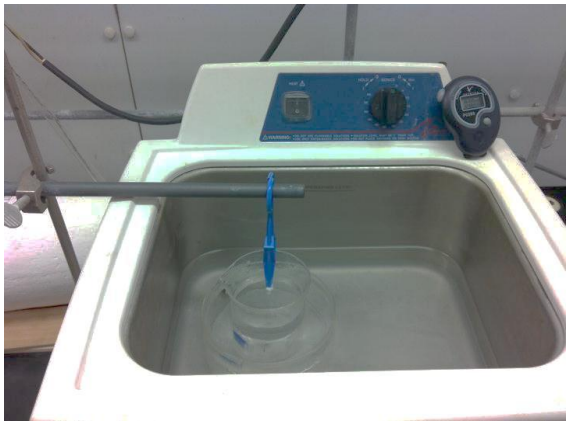

Fig. 2.3 The configuration of CBD.

2.1.3 Rapid thermal process (RTP)

RTP is a thermal process, which usually applied to modify electrical properties of films or activate dopant. The RTP (DMS) used in this study (Fig. 2.4) is occupied with four temperature sensors inside a chamber, those establish the temperature profile targeted and two temperature sensors on the quartz sample stage for monitoring. The tungsten filaments have been used as heating sources.

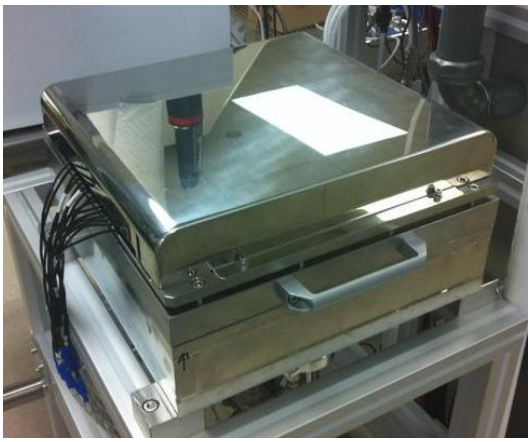

Fig. 2.4 The image of rapid thermal process

2.2 Fabrication of semi-transparent heterojunctions

In the field of organic-based semi-transparent solar cell, it has weaknesses of degradation issue and low efficiency. For inorganic type of the cells, people have successfully fabricated cells with assistance of thermal treatment. However, none of the working cells are fabricated without extra thermal budge. In this study, we were attempting to fabricate Cu_2O/AZO heterojunction solar cells at low temperature. In addition, both CBD and sputtered buffer layer: i-ZnO shows its effect for improvement of junction performance.

2.2.1 Preparation of glass substrates

For targeted structure of the semi-transparent solar cell, glasses were utilized as substrates. It is important to ensure the cleanness of glass because photogenerated electron-hole pairs are very sensitive to impurities. The glasses were ultrasonicated inside toluene, acetone, and isopropyl alcohol in sequence. Finally, the cleaning process was done with drying by nitrogen. Those cleaning steps can remove all organic substances on glasses.

2.2.2 Sputtered deposition of ITO, AZO and Cu_2O

On top of the clean glass, indium tin oxide (ITO) was deposited from a 99.99% pure ITO target (SCM) using a RF sputter. Subsequently, different sequences of AZO and Cu_2O films

were deposited from a 99.90% pure ZnO/Al_2O_3 (2 wt%) target and 99.9% pure Cu_2O target respectively on top of ITO-coated glass by the RF sputter as well. Finally, the junction was completed by depositing a fork shape Al or Cu electrodes on top of the junction using a thermal evaporator. Table 2.1 summarizes the deposition conditions of ITO, AZO and Cu_2O.

Table 2.1 Sputter deposition of ITO, AZO and Cu_2O

Target	Working pressure (mtorr)	Ar flow rate (sccm)	RF power (W)	Thickness (nm)	Dep. time (min)
Cu_2O	10	15	500	210	5
ZnO/Al_2O_3 (2 wt. %)	4	7	100	440	40
ITO	6	20	200	300	20

2.2.3 Deposition of intrinsic ZnO as a buffer layer in the heterojunction

In order to investigate the effect of different i-ZnO fabricated by different technologies the sputtered i-ZnO and CBD deposition of intrinsic ZnO (i-ZnO) were inserted between AZO/Cu_2O as buffer layer respectively.

2.2.3.1 Sputter i-ZnO

The sputtered i-ZnO films were deposited by RF sputtering. The thicknesses were varying from 10 nm to 50 nm. Table 2.2 summaries detail of sputtered i-ZnO films.

Table 2.2 Summary of sputtered i-ZnO

Target	Working pressure (mTorr)	Ar flow rate (sccm)	RF power (W)	Thickness (nm)
i-ZnO	3	150	200	10
				20
				100

2.2.3.2 Chemical bath deposition of i-ZnO

First of all, preparing zinc acetate solution for 150 ml at the concentration of 0.019M, and heat up to 50°C. Secondly, placing the substrate into solution, and adding desired amount of ammonia into solution. Thirdly, well mix the solution by magnetic stirring bar during the process. Finally, the i-ZnO films have been completed.

For the deposition of CBD i-ZnO, it is made from a aqueous solution of zinc acetate ($Zn(CH_3COO)_2$) and ammonia (NH_4OH) at 50 ^oC according to the procedure published previously [41]. We did perform ultrasonication simultaneously in order to obtain more uniform i-ZnO films. Table 2.3 summarizes two different i-ZnOs prepared for the study. The thickness of CBD deposited i-ZnO film was about 50 nm.

Table 2.3 Variables used for the CBD of i-ZnO.

pH	Conc. of zinc acetate (M)	Conc. of ammonia (M)	Bath Temperature (°C)	Deposition time (min)	Usage of ultrasonication during deposition
8.7	0.019	0.05	50	50	No
10		0.44			Yes

2.3 Morphology and structure analyses of thin-films

2.3.1 Scanning Electron Microscope

In order to analyze the morphology of the films, a variable pressure SEM (Hitachi S-3000N) at the Characterization Center for Materials & Biology (CCMB) of the University of Texas at Arlington was utilized (Fig. 2.5). S-3000N is equipped with a tungsten hairpin type filament as an electron source. It has the capability to go down to 3 nm in resolution at high vacuum mode. The magnification varies from 15X to 300,000X. The images of insulating materials are also realized at low vacuum mode without any conductive coating on the sample in the back-scattered mode. In addition, energy-dispersive X-ray spectroscopy (EDS) is also attached allowing users doing composition analysis.

Fig. 2.5 Hitachi S-3000N scanning electron microscope (SEM) at UTA CCMB.

2.3.2 X-ray diffraction (XRD) for structural analysis

XRD was employed to analyze the crystal structure of films as well as information of grain size. D-500 (Siemens) at CCMB (is used and it is equipped with a Cu Kα source (Fig. 2.6). Diffraction was performed using a θ-2θ scan and PCPDFWIN software was used to identify diffraction peaks and phases.

Fig. 2.6 D-500 (Siemens) X-ray Diffractometer.

2.4 I-V characterization of the heterojunctions

A custom-made I-V probe station equipped with an AM 1.5 standard white light is used to characterize the heterojunctions. The four-point probe configuration was used in order to

prevent inaccurate measurement from the potentially high contact resistance. The device can be measured under light and the data analysis can provide V_{OC}, J_{SC}, FF, and PCE.

CHAPTER 3

RESULTS AND DISCUSSION

3.1 Competitive nucleation rate and the effect of solution pH in CBD of i-ZnO

3.1.1 Effect of substrates

Fig. 3.1 shows the i-ZnO films deposited, using CBD, on top of several substrates including bare glass, Si wafer, and AZO/ITO/glass when ammonia concentration was low - the pH value of the bath was 8.5. The deposition of non-uniform mixed particles occurred on every substrate except for AZO/ITO/glass. The particles were thought to be deposited $Zn(OH)_2$. In the reaction at low pH, homogeneous nucleation of $Zn(OH)_2$ in the chemical bath dominated the reaction and the particle deposition of $Zn(OH)_2$ on the substrate occurred. The detailed analyses of the chemical reaction will be shown in the next section. On the other hand, i-ZnO film formed on top of AZO possibly because the presence of AZO on the substrate made the heterogeneous nucleation of i-ZnO on top of AZO much faster than both the homogeneous nucleation rate of $Zn(OH)_2$ in the bath and subsequent deposition rate of $Zn(OH)_2$ particles.

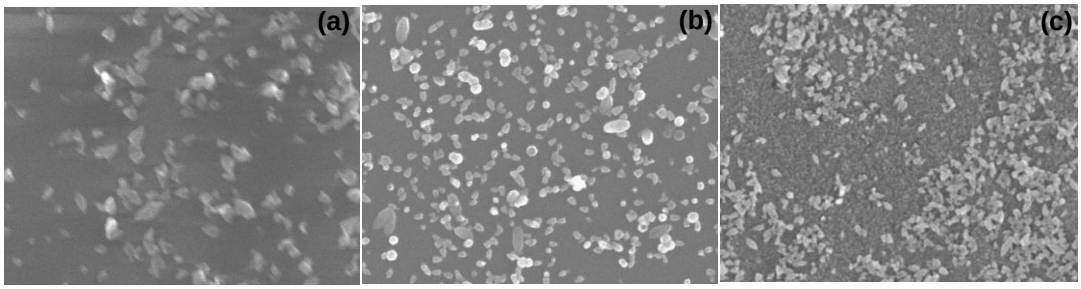

Fig. 3.1 The SEM images of film deposited at low pH value on
(a) bare glass, (b) Si wafer and (c) AZO coated glass.

Although $Zn(OH)_2$ particles still existed on top of AZO, its density was much lower than that of $Zn(OH)_2$ particles on top of other substrates. In short, the hypothesis is that the growth rate of

heterogeneous ZnO was enhanced by assistance of AZO underneath. However, the uniformity of heterogeneous ZnO was still bad due to the adhesion of $Zn(OH)_2$ particles.

3.1.2 Effect of solution pH value

A series of reactions below explains the possible reaction route of forming i-ZnO in the process of chemical bath deposition (schemes 3.1) [42].

$$Zn(CH_3COO)_2 + 2NH_4OH \rightarrow Zn(OH)_2 + 2NH_4(CH_3COO)$$

$$Zn(OH)_2 + 4NH_4OH \rightarrow Zn(NH_3)_4(OH)_2 + 4H_2O$$

$$Zn(NH_3)_4(OH)_2 \rightarrow Zn(NH_3)_4^{+2} + 2OH^-$$

$$Zn(NH_3)_4^{+2} + 2OH^- \rightarrow ZnO + NH_3 + 2H_2O$$

Scheme 3.1 A series of chemical reaction for CBD i-ZnO [42].

Overall, the formation of the complex, $Zn(NH_3)_4(OH)_2$ has been found as the key factor to deposit ZnO compound through the process. As expected from the scheme, the formation of $Zn(NH_3)_4(OH)_2$ will be preferred when the concentration of ammonia is relatively high and ZnO will eventually form. Meanwhile, $Zn(OH)_2$ will become the main product when the ammonia concentration is low. For this reason, the different samples were prepared with higher ammonia concentrations expecting preferred of ZnO formation.

SEM micrographs (Fig.3.2) showed the series samples of CBD i-ZnO deposited with different pH of solution. Samples (a) and (b) showed CBD-deposited *i*-ZnO on top of the sputter-deposited AZO. The larger grains (particles) appeared in sample (a) were possibly originated

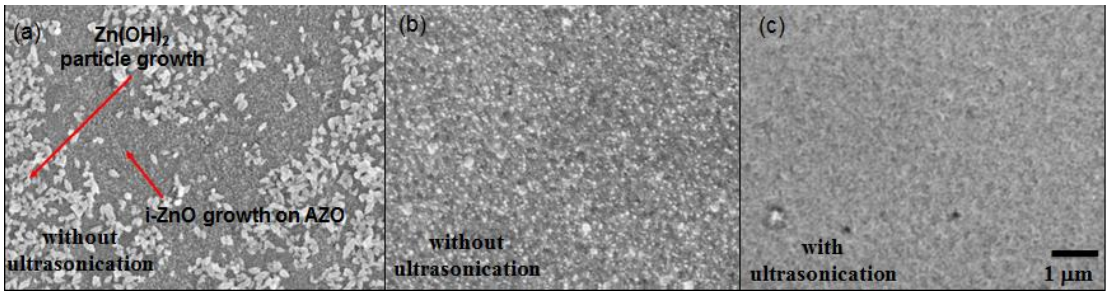

Fig.3.2 SEM micrographs of i-ZnO: (a) CBD (pH=8.5) i-ZnO, (b) CBD (pH=10) i-ZnO, and (c) CBD (pH=10) i-ZnO with ultrasonication.

from the deposition of $Zn(OH)_2$ particles generated inside the bath solution through a homogeneous nucleation at low ammonia concentration. pH was equal to 8.5 in this case. In contrast, Sample (b) was deposited at high concentration of ammonia - pH of the solution was 10 - and, the deposition showed more uniform films with minimal $Zn(OH)_2$ particles. Sample (c) was identical to Sample (b) except that the ultrasonication was employed during the deposition in order to further reduce the adherence of $Zn(OH)_2$ particles on the sample surface.

In short, low pH value of solution exhibited homogeneous $Zn(OH)_2$ preferring chemical reaction. In contrary, high pH solution had dramatically increased heterogeneous growth of ZnO and reduced homogeneous $Zn(OH)_2$ particles. Furthermore, the formation of $Zn(OH)_2$ is inevitable. Therefore, ultrasonication was performed in order to remove $Zn(OH)_2$, and further improve homogeneity of ZnO films.

3.1.3 X-ray diffraction analysis on the ZnO thin-films

All the XRD patterns of AZO coated glass and CBD i-ZnO on top of sputtered AZO (Fig. 3.3) showed a single diffraction peak at about 34.5°. While the peak from Sample (a) clearly represents (002) of wurtzite ZnO with a hexagonal structure, it should be noted that the diffraction (200) of orthorhombic $Zn(OH)_2$ and (006) of hexagonal $Zn(OH)_2$ can occur at the very similar diffraction angle complicating the analysis of Samples (b) and (c). The slightly increase in the full-width-at-half-maximum (FWHM) of the peak from Sample (b) can be hypothetically attributed to the disorder of $Zn(OH)_2$ particles deposited on the surface of AZO. Further analysis, however, is necessary to directly understand the chemical identity of the film deposited in Sample (b). The intensity of the peak from Sample (c) was very small because CBD i-ZnO was uniformly covering up AZO and it is very difficult to make further analysis. In contrary, the intensity of the peak from Sample (b) was lower than Sample (c), which can be attributed to thinner and sparser i-ZnO films obtained from lower pH of the solution. The thickness of *i*-ZnO was around 50 nm in Sample (c).

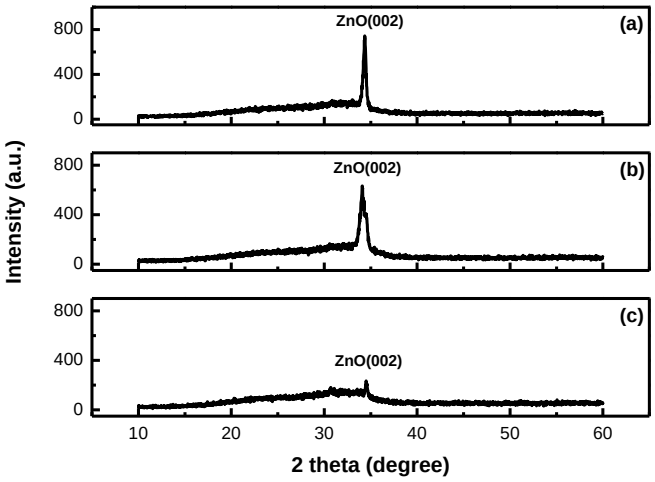

Fig. 3.3 XRD obtained from the samples: (a) sputtered AZO, (b) CBD (pH=8.5) i-ZnO on top of sputtered AZO, (c) CBD (pH=10) i-ZnO with ultrasonication on top of sputtered AZO

3.1.4 Analysis of Cu_2O annealed using a rapid thermal annealer

As-deposited Cu_2O shows very high resistance. In order to improve the carrier transport in bulk Cu_2O, the completed device (Cu_2O/sputtered i-ZnO/AZO) was annealed at 350^oC for 30 min under vacuum. Fig. 3.4 showed SEM images of Cu_2O as-deposited and annealed. The as-

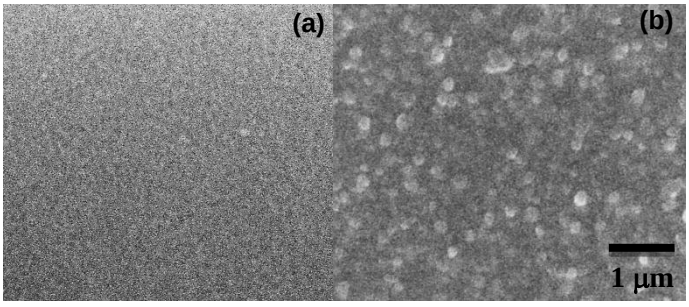

Fig. 3.4 SEM images of Cu_2O. (a) as-deposited and (b) annealed at 350^oC for 30 min.

deposited Cu_2O revealed tiny and obscure grains structure, which is reasonable for high resistance. On the other hand, the grain structure of annealed become significant (Fig. 3.4). In

addition, Fig. 3.5 showed XRD profiles of Cu_2O before and after annealing. We had noticed that the FWHM of Cu_2O (111) peak had become smaller for sample after annealing, which indicates the grain size of Cu_2O had enlarged. Furthermore, other peaks of Cu_2O were presented, which provides further evidence to the improvement of crystallinity of Cu_2O accordingly.

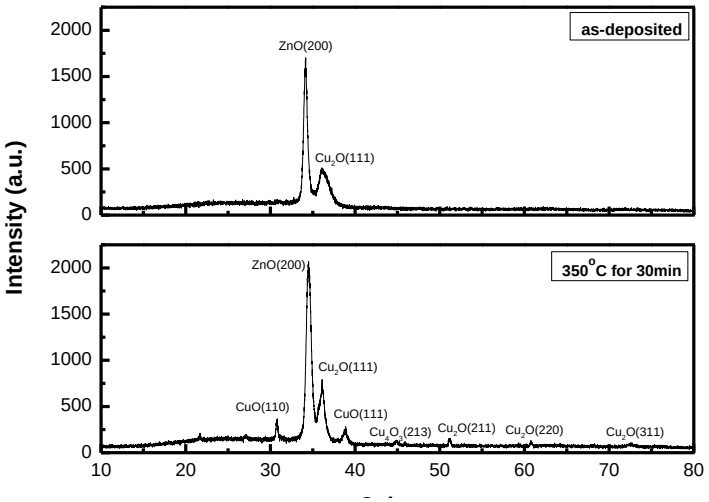

Fig. 3.5 XRD profiles of Cu2O/sputtered i-ZnO/AZO/glass

3.2 Analysis of the heterojunction

3.2.1 I-V characteristics

Dark I-V measurements on the heterojunctions (Fig. 3.6) clearly exhibit that the AZO/Cu_2O without the presence of *i*-ZnO film shows an ohmic behavior. This indicates no P-N junction forming at this structure, which means no rectifying phenomena. On the other hand, AZO/Cu_2O heterojunctions with *i*-ZnO show rectification characteristics regardless of the deposition methods of *i*-ZnO. The detail will be discussed as following sections:

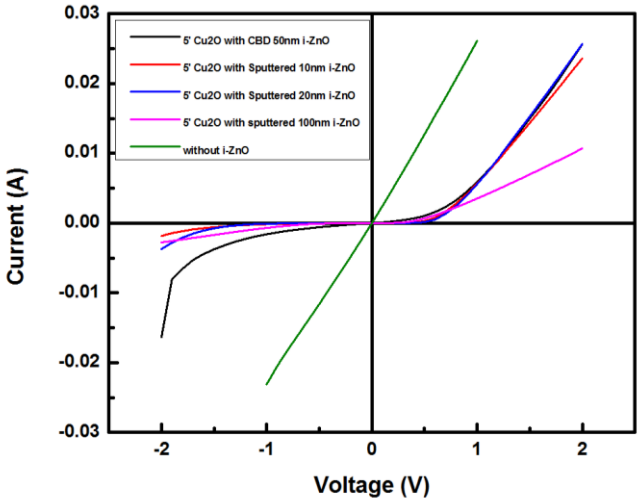

Fig. 3.6 Dark I-V characteristics of AZO/i-ZnO/Cu_2O heterojunctions with different i-ZnO buffer layer.

3.2.2 Role of the buffer layer: i-ZnO

The junction without i-ZnO expectedly has more defects at the interface (Fig. 3.7 (a)), which originated from the plasma damage caused by the subsequent Cu_2O sputter process. In contrary, the junction with insertion of intrinsic buffer layer reduced the defects at the interface as shown in Fig. 3.7(b). In other words, interface defects states provide shunting path to carriers, and results in lower cell performance. In addition to defects issue at the junction interface, the tunneling effect, which electrons tunnel through from conduction band of AZO to valance band

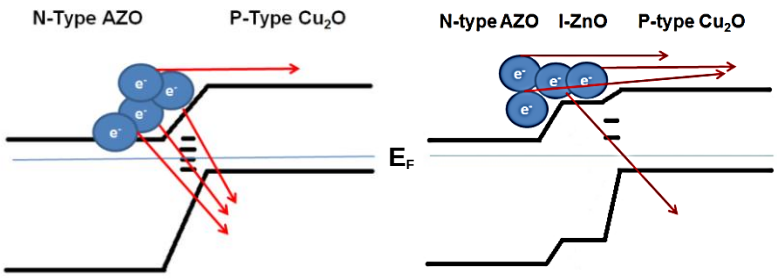

Fig 3.7 Carrier transport across junction when the density of interface defects is (a) low and (b) high.

of Cu_2O, has played an important role to cell performance as well. It has been reduced by insertion of i-ZnO because the distance between conduction band of AZO and valence band of Cu_2O is enlarged for the device with the presence of i-ZnO. Hence, the probability of tunneling effect will be eliminated as shown in Fig. 3.7(b).

3.2.3 The effect of deposition technologies

The device with the sputtered and CBD i-ZnO both show comparable results (Fig. 3.6) by comparing threshold voltages (V_{th}). V_{th} is around 0.5 Volts for both 50nm CBD and 10nm sputtering cases. When applied voltage exceeds V_{th}, the diode turns on and the appreciable amount of forward current emerges as charge carriers are able to overcome the reduced barrier due to forward bias and move from n side to p side (Fig. 3.8). In addition, i-ZnO from a sputter was deposited at RF power of 200 W, which is lower than the power for Cu_2O, 500W. Hence, the defects from process of sputtered i-ZnO will be much less than sputtered Cu_2O. That is the reason why both CBD and sputtered i-ZnO can both protect AZO from subsequent Cu_2O deposition.

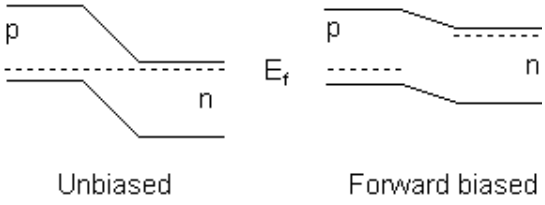

Fig. 3.8 P-N junction at forward bias [43].

3.2.4 The effect of i-ZnO thickness

From Fig. 3.6, we have discovered that current become smaller when intrinsic layer gets thicker at forward bias. That can be ascribed to increment of series resistance originating from thicker i-ZnO films. The resistance of i-ZnO is expected to be high because base pressure of the sputter system used is about 10^{-6} torr, under which oxygen-sufficient ZnO will be

generally deposited and the concentration of V_O is expected to be low resulting in the low conductivity of i-ZnO [44].

3.2.5 The lattice mismatch

The lattice mismatch (Δa) between AZO and Cu_2O could be calculated through eq. 3.1 [45].

$$\Delta a = 2(a_2 - a_1) / a_2 + a_1 \qquad \text{(eq. 3.1)}$$

where a_1 = 3.30 (Å) [30-q], a_2 = 4.27 (Å) [46] are the lattice constant of AZO and Cu_2O, respectively. The Δa is about 25.6%, which is large lattice mismatch. Although insertion of i-ZnO has reduced some defects from plasma damages, the AZO/Cu_2O heterojunction intuitively possess certain numbers of defects at the interface. As the result, the fundamental limitation constrains the performance of cell. However, the cell could be enough for certain applications, such as LC attenuator devices.

3.2.6 Performance of cell under light

The photovoltage of the junction under light is currently very small, which can be attributed to several hypotheses, such as high defect density and tunneling effect. Another reason could be short minority carrier diffusion length in the Cu_2O thin-film. Therefore, we had tried annealing the device at 350^oC, and crystallinity of Cu_2O had clear improvement as showed in section 3.1.4. However, annealed device had showed ohmic behavior (not shown) under dark I-V characterization. This result can be attributed to dopant diffusion across buffer to either direction, so that potential barrier between AZO/Cu_2O has disappeared. The bulk properties of AZO and Cu_2O have been modified.

CHAPTER 4

CONCLUSION

The working heterojunction of AZO/i-ZnO/Cu_2O was successfully fabricated at low temperature by employing either a CBD-deposited or sputter-deposited i-ZnO buffer layer at the junction interface of AZO/Cu_2O. For CBD of i-ZnO, the pH of the bath solution has been confirmed as the key variable to form a uniform film of i-ZnO and the high concentration of ammonia in the solution reduced the formation of $Zn(OH)_x$ particles in the solution and their deposition on the growing surface and relatively increased the nucleation rate of ZnO on AZO at the same time. Further improvement in the uniformity of i-ZnO film was accomplished by using ultrasonication during the deposition preventing the adhesion of the particles. The effect of buffer layer on the performance of the heterojunction was studied as well. The insertion of i-ZnO can prevent plasma damage from subsequent Cu_2O deposition. Also, intrinsic layer can be a tunneling effect reducer when junction is at forward bias. The junction with thinner sputtered i-ZnO actually shows better rectifying junction formation than thicker case through analysis of I-V characteristics. In addition, annealed device had a trade-off effect. The crystallinity of absorber got better, on the other hand, the properties of both AZO and Cu_2O may become worse than as-fabricated device. In short, the lack of photovoltage needs to be further investigated. Several hypotheses can be established including the short diffusion length in Cu_2O, high surface recombination at air/Cu_2O top surface, and the higher defect density at the junction due to lattice mismatch.

CHAPTER 5

FUTURE WORK

The performance of device under light still needs to be improved. Several approaches can be attempted.

1. High recombination rate of Cu_2O surface

   Cu_2O is currently on the top of device. In this configuration, high surface recombination could happen at air/Cu_2O top surface. Therefore, the surface recombination could be suppressed by depositing Cu_2O first and then AZO will be the top layer, which is superstrate structure.

2. Short minority carrier diffusion length in bulk Cu_2O

   As previously shown in Fig. 3.4, the grain size of as-deposited Cu_2O was very tiny. This can be the cause of short carrier diffusion length. The grain structure of Cu_2O has been improved significantly after annealing. However, it is not possible to prevent the diffusion of dopant with current cell structure if they do. Therefore, annealing Cu_2O individually can be achieved by depositing Cu_2O first on ITO glass. In this way, the improvement of Cu_2O structure can be made, and the property of AZO can be maintained. Thinner Cu_2O layer is another option to overcome short carrier diffusion length. The minority carriers may be more efficiently extracted due to thinner Cu_2O films.

REFERENCES

[1] Environmental transport association, “Transparent solar panels for car windscreens”. October 2011, [online]. Available at: http://www.eta.co.uk/2011/10/07/transparent-solar-panels-car-windscreens

[2] Engineering and technology magazine, “Semi-transparent solar glazing panels”. July 2011, [online]. Available at: http://expresstougheningnews.wordpress.com/2011/07/25/more-glass-news/

[3] AlphaMicron (AMI) ,“UVISION Variotronic Ski Goggle”. [online]. Available at: http://www.alphamicron.com/consumer/fx_variotronic_ski_goggles.html

[4] R. R. Lunt and V. Bulovic, Applied Physics Letters 98, 113305 (2011)

[5] Y. Nishi, T. Miyata, J. Nomoto, and T. Minami, *Proc. of 37th IEEE PVSC* (2011).

[6] G.K. Paul, R. Ghosh , S.K. Bera, S. Bandyopadhyay, T. Sakurai, K. Akimoto, Chemical Physics Letters, 463, (2008), 117-120.

[7] D.K. Zhang, Y.C. Liu, Y.L. Liu, H. Yang, Physica B 351 (2004) 178–183

[8] Jin Young Moon, Jun Ho Kim, Hyunghoon Kim, Ho Seong Lee, Young Yi Kim, Hyung Koun Cho, Hong Seung Kim, *Thin Solid Films* 517, (2009), 3931.

[9] I. Repins, M.A. Contreras, B. Egaas, C. Dehart, J. Scharf, C. L. Perkins, B. To, and R. Noufi, *Prog. in Photovolt.* 16, (2008), 235.

[10] A. Yamada, H. Miyazaki, Y. Chiba, M. Konagai, *Thin Solid Films* 480–481, (2005), 503.

[11] T. Yoshida, S. Fujikake, Fuji Electric Review, Vol. 49, No.2. (2003)

[12] International Energy Agency, key world energy statistics, (2011)

[13] Canberra Times. “More to do to help people go solar”. Nov 16 2007, p. 1

[14] M. A. Green, K. Emery, Y. Hishikawa and W. Warta, Prog. Photovolt: Res. Appl. 2011; 19:84–92

[15] “Working of photovoltaic cells – solar cells”. [online]. Available at: http://www.solarpowernotes.com/how-solar-cells-works.html

[16] Swiss federal laboratories for materials science and technology, “Swiss researchers set new world record for solar cells”, May 2011, [online]. Available at: http://www.sccij.jp/news/overview/detail/article/2011/05/23/swiss-researchers-set-new-world-record-for-solar-cells/

[17] Konarka, “Ink Jet Solar Cells”. March 2008. [online]. Available at: http://www.konarka.com/index.php/site/pressreleasedetail/konarka_announces_first_ever_demonstration_of_inkjet_printed_solar_cells

[18] J. Nelson, “The physics of solar cells”, (2003)

[19] B. Curtin, R. Biswas and V. Dalal, Applied Physics Letters 95, 231102 (2009)

[20] P. Stallinga, Universidade do Algarve,“Theory of electrical characterization of (organic) semiconductors”. December 2009, [online]. Available at: http://ceot.ualg.pt/OptoEl/theory/2terminal/

[21] H. Lund, R. Nilsen, O. Salomatova, D. Skåre, E. Riisem, “Solar cells”. 2008, [online]. Available at : http://org.ntnu.no/solarcells/pages/introduction.php

[22] http://www.sciencedirect.com/science/article/pii/0927024895800042

[23] Electronic Materials Research Group at MIT, “Light Trapping for Thin Film Solar Cells”. Available at: http://photonics.mit.edu/Solar_Cells_Light_Trapping.html

[24] Martin A. Green, J Mater Sci: Mater Electron (2007) 18:S15–S19

[25] R. Biswas, I. Kwon, and C. M. Soukoulis, Physical Review B, Vol. 44, No. 7 (1991)

[26] T. Takamoto, T. Agui, A. Yoshida, K. Nakaido, H. Juso, K. Sasaki, K. Nakamora, H. Yamaguchi, T. Kodama, H. Washio, M. Imaizumi, and M. Takahashi, Photovoltaic Specialists Conference (PVSC), 2010 35th IEEE, 412-417.

[27] P. Jackson, D. Hariskos, E. Lotter, S. Paetel, R. Wuerz, R. Menner, W.Wischmann, M. Powalla, New world record efficiency for Cu(In,Ga)Se2 thin-film solar cells beyond 20%.

Prog. Photovolt. January 2011 [online]. Available at: http://dx.doi.org/10.1002/pip.1078

[28] A. Chiril, S. Buecheler, F. Pianezzi, P. Bloesch, C. Gretener, A. R. Uhl, C. Fella, L. Kranz, J. Perrenoud, S. Seyrling, R. Verma, S. Nishiwaki, Y. E. Romanyuk, G. Bilger and A. N. Tiwari, 10.1038/NMAT3122, (2011)

[29] T. Minami, T. Miyata, K. Ihara, Y. Minamino, and S. Tsukada, *Thin Solid Films* 494, (2006), 47.

[30] Ü. Özgür, Ya. I. Alivov, C. Liu, A. Teke, M. A. Reshchikov et al., J. Appl. Phys. 98, 041301 (2005)

[31] C. G. Van de Walle, Physica B 308–310, 899 (2001).

[32] S. L. Ou, D. S. Wuu, S. P. Liu, Y. C. Fu, S. C. Huang, and R. H. Horng, Optics Express, Vol. 19, No. 17 (2011)

[33] T. Terasako, M. Yagi, M. Ishizaki, Y. Senda, H. Matsuura, S. Shirakata, *Surf. Coat. Technology,* 201, 8924 (2007)

[34] G.K. Paul, R. Ghosh , S.K. Bera, S. Bandyopadhyay, T. Sakurai, K. Akimoto, Chemical Physics Letters, 463, (2008), 117-120.

[35] B. M. Ataev, A. M. Bagamadova, A. M. Djabrailov, V. V. Mamedo, and R. A. Rabadanov, Thin Solid Films 260, 19 (1995).

[36] B. P. RAI, Solar cells, 25 (1988) 265-272

[37] A. A. Ogwu, T. H. Darma, and E. Bouquerel, *J. of Achievements in Materials and Manufacturing Engineering* 24, (2007), 1.

[38] H. Raebiger, S. Lany, and A. Zunger, Physical Review B 76, 045209 (2007).

[39] D.K. Zhanga, Y.C. Liu, Y.L. Liu, H. Yang, Physica B 351, (2004), 178–183.

[40] T. C. Grove, Advanced Energy Industries, Inc., “Arcing problems encountered during sputter deposition of aluminum” [online]. Available at: http://www.advanced-energy.com/upload/File/White_Papers/SL-WHITE5-270-01.pdf

[41] Hisashi Miyazaki, Rui Mikami, Akira Yamada, and Makoto Konagai, *Jap. J. of Appl. Phys.*

45, (2006), 2618.

[42] Tapas K Chaudhuri and Anjana Kothari, J. of Optoelectronic and Biomedical Mater. Vol. 1, Issue 1, P. 20-24, (2009).

[43] MATTER, University of Liverpool. [online]. Available at: http://www.matter.org.uk/glossary/detail.asp?dbid=168

[44] J.Lee, K. H. Kang, S. K. Kim, K. H. Yoon, I J. Park, J. Song, Solar Energy Materials & Solar Cells 64 (2000) 185~195.

[45] R. A. Ismail, Journal of semiconductor technology and science, Vol. 9, No. 1, March 2009.

[46] L.S. Yu, in: Y.F. Li (Ed.), Physics of Semiconductor Heterojunction, Science Press, Beijing, 1990.

BIOGRAPHICAL INFORMATION

Yu-Nung Huang received his Bachelor of Engineering Degree in Materials Science and Engineering Department from I-Shou University, Taiwan, in June 2005. After finished military service, he pursued the Master Degree in Department of Materials Science and Engineering at the University of Texas at Arlington (UTA) since early 2010. He has joined Photovoltaic Materials Laboratory, which is supervised by a young passionate professor, Dr. Michael Jin from UTA. In addition, he has been involved in projects including CIGS thin film solar cell and Smart Windows: Semi-Transparent Photovoltaic Devices. After graduation, he would like to extend his career and contribute his knowledge of photovoltaic into the industry and society.